Modeling the sequential dissociative double ionization of math xmlns="http://www.w3.org/1998/Math/MathML">msub>mi mathvariant="normal">O/mi>mn>2/mn>/msub>/math> by ultrashort intense infrared laser pulses

C. H. Yuen, P. Modak, Yan Song, Song-Feng Zhao, and C. D. Lin

Modeling the Sequential Dissociative Double Ionization of O_2 by Ultrashort Intense Infrared Laser Pulses

C. H. Yuen,[1, *] P. Modak,[1] Yan Song,[2] Song-Feng Zhao,[2] and C. D. Lin[1, †]

[1]*J. R. Macdonald Laboratory, Department of Physics,*
Kansas State University, Manhattan, Kansas 66506, USA
[2]*Key Laboratory of Atomic and Molecular Physics and Functional Materials of Gansu Province,*
College of Physics and Electronic Engineering, Northwest Normal University, Lanzhou, 730070, China

(Dated: January 11, 2023)

A density matrix approach for sequential double ionization (DM-SDI) of molecules has been developed recently and was applied to the N_2 molecule [Yuen and Lin, Phys. Rev. A 106, 023120 (2022)]. In this article, we extended the DM-SDI model to O_2, which is a more complicated system to model than N_2, due to its electronic structures and spin-orbit and laser couplings in the manifold of doubly charged states. We obtained a good agreement on the kinetic energy release spectrum of $O^+ + O^+$ from previous experiments. Thanks to the low computational cost of the model, we explored the mechanism behind the ionization and dissociation dynamics as well as the effects of lasers on the spectrum. This work will pave the way to model sequential dissociative double ionization of larger molecules and to probe molecular dynamics by measuring kinetic energy release spectra from this process.

I. INTRODUCTION

Molecular breakup due to strong field sequential double ionization (SDI) could be a promising probing scheme for molecular dynamics, since intense femtosecond infrared (IR) laser pulses and coincidence measurement setup are widely available [1–11]. However, the lack of theoretical support has made this probing scheme unfeasible so far. Recently, we developed a density matrix approach for SDI of molecules and applied it to the case of N_2 [12]. For brevity, we refer this model as the DM-SDI model hereafter. We showed that our simulated kinetic energy release (KER) spectrum for the dissociation of $N^+ + N^+$ agrees excellently with the experiment by Voss *et al.* [13], thus opening up the possibility on simulating SDI of more complicated targets. To increase the complexity of the target, in this article, we extend the DM-SDI model to the O_2 molecule.

SDI of O_2 is more difficult to model due to its open-shell electronic structure, $^3\Sigma_g^- : \ldots 3\sigma_g^2 1\pi_u^4 1\pi_g^2$, at the neutral ground state. In the single active electron picture, ionizing a spin up or down electron from its occupied orbital will then lead to two different electronic spin states at different energies. Consequently, one has to treat the spin up or down electron differently instead of indistinguishably. Further ionizing the system leads to a more interesting scenario: Removing a π_u electron from the $X^2\Pi_g(3\sigma_g^2 1\pi_u^4 1\pi_g^1)$ state of O_2^+ could lead to formation of different electronic states, in which their energies can be different by about 3 eV. As a result, the binding energies of such orbitals are not clearly defined. Since strong field ionization is a non-linear process, the ionization rate is highly sensitive to the binding energy.

The ambiguity in the binding energy thus poses a severe problem to single active electron models for tunneling ionization such as the MO-ADK theory [14]. One of the main goal of this article is to address this situation with a general approach.

There are several experimental investigations about or related to the double ionization of O_2 by intense ultrashort IR laser pulses. These include nonsequential double ionization of O_2 [13, 15–18], Coulomb explosion [19–22], and strong field ionization of O_2^+ [23]. Most importantly, there are data on SDI of O_2 from Voss *et al.* [13] and Wu *et al.* [24], which we can compare our simulated results with. In addition, there are other relevant studies of O_2 such as Doppler free KER spectrum [25] and predissociation rates [26] of O_2^{2+}, which provide insights on O_2^{2+} dissociation dynamics. There is also an investigation on normal Auger electron spectrum of O_2 by Bao *et al.* [27], which gives accurate vertical ionization potentials of the triplet O_2^{2+} states.

While SDI of O_2 has not been investigated theoretically, there are some work on the interaction of strong IR laser pulses with O_2 or O_2^+. Thumm and coworkers investigated the nuclear dynamics of O_2^+ after strong field ionization of O_2 [28] and strong field dissociation of O_2^+ [29, 30]. There are also studies focused on vibronic couplings and coherence in O_2^+ after strong field ionization of O_2 [31–33]. Last but not least, there are extensive studies on the electronic structure of O_2 and O_2^+, for examples, see Refs. [34–36].

In this article, we extended the DM-SDI model to O_2 by introducing the effective binding energy for states with degenerate electronic configurations and including the laser couplings between the doubly charged states. The extended DM-SDI model reproduces the experimental KER spectra of $O^+ + O^+$ from Voss *et al.* [13] and Wu *et al.* [24] very well. We also showed that the above extensions of the DM-SDI model are necessary to reproduce the experimental spectra by comparing spectra cal-

culated from different models. Prediction on the wavelength, alignment, and laser intensity dependence of the KER spectra are given and discussed.

This article is arranged as follows: In the next section, we first briefly review the DM-SDI model and extend it to O_2. We then discuss the assignment of binding energies of O_2^+ orbitals. We close the section with computational details about the electronic structure. In Sec. III, we present our main results and compare it with the experiment by Voss *et al.* [13] and Wu *et al.* [24]. In Sec. IV, we explore the mechanisms behind O_2 SDI, compare results from different models, and investigate effects from different laser parameters on the KER spectra. Finally, we summarize the results and give outlook for future research in Sec. V.

II. THEORETICAL APPROACH

A. The DM-SDI model

The model we used for O_2 SDI is based on a density matrix approach where the neutral, ionic, and doubly charged states are treated as different open systems. Details about the DM-SDI model are described in our previous article [12].

Briefly, in the model, nuclei of the the molecule are assumed to be fixed during the ionization process. The tunneling ionization from the neutral and the ionic states are described by the MO-ADK theory [14], and the ionized electrons are neglected such that different charge states are incoherent. In addition, for states with the same charge, different electronic states are populated incoherently from the tunneling ionization, but the laser couples those states coherently. For some reasons which we will explain later in this section, for the O_2 system, we include laser couplings between the doubly charged states, leading to the set of equations of motion for the density matrices $\rho^{(i)}$,

$$\frac{d\rho^{(0)}}{dt} = -\sum_i \rho^{(0)}(t)W_i^{(0)}(t),$$

$$\frac{d\rho^{(1)}}{dt} = -\frac{i}{\hbar}[H^{(1)}, \rho^{(1)}] + \Gamma^{(1)}(t),$$

$$\frac{d\rho^{(2)}}{dt} = -\frac{i}{\hbar}[H^{(2)}, \rho^{(2)}] + \Gamma^{(2)}(t), \qquad (1)$$

where $i = 0, 1, 2$ denote the neutral, ionic, and doubly charged states. $W_i^{(0)}$ is the ionization rate from the neutral ground state to the ith ionic state. The Hamiltonian $H^{(i)} = H_0^{(i)} + \vec{d} \cdot \vec{E}$, where $H_0^{(i)}$ is the field-free Hamiltonian, with $\vec{d}$ being the dipole moment and $\vec{E}$ being the

TABLE I. Experimental vertical ionization potential (I_p) to the O_2^+ states [36] and structure parameters of the O_2 orbitals for MO-ADK tunnel ionization rates [37]. The orbital angular momenta l and the corresponding structure factors C_{lm} are listed for each orbital. For a π or σ orbital, $m = 1$ or 0.

States	Config.	I_p (eV)	l	C_{lm}
$X^2\Pi_g$	$1\pi_g^{-1}$	12.3	$\{2, 4\}$	$\{0.69, 0.06\}$
$a^4\Pi_u$	$1\pi_u^{-1}$	16.7	$\{1, 3, 5\}$	$\{1.86, 0.36, 0.02\}$
$b^4\Sigma_g^-$	$3\sigma_g^{-1}$	18.2	$\{0, 2, 4\}$	$\{3.49, 2.06, 0.25\}$

laser field. The source terms $\Gamma^{(1)}$ and $\Gamma^{(2)}$ are

$$\Gamma_{ij}^{(1)}(t) = \delta_{ij}\left[\rho^0(t)W_i^{(0)}(t) - \sum_n \rho_{ii}^{(1)}(t)W_{n\leftarrow i}^{(1)}(t)\right],$$

$$\Gamma_{mn}^{(2)}(t) = \delta_{mn}\sum_i \rho_{ii}^{(1)}(t)W_{n\leftarrow i}^{(1)}(t),$$

where $W_{n\leftarrow i}^{(1)}$ is the ionization rate from the ith ionic state to the nth doubly charged state. Setting the initial condition to be $\rho^{(0)}(t_0) = 1$ and $\rho^{(1)}(t_0) = \rho^{(2)}(t_0) = 0$, we solve Eq. (1) by the classic Runge-Kutta method and obtain population of all the states at the end of the laser pulse.

The most important input in our model is the MO-ADK ionization rates [14], which strongly depend on the symmetry of the ionized orbital and its binding energy. Such information is obtained from electronic structure calculations [37, 38]. The electronic structure at the equilibrium geometry of O_2 ($R = 1.21$ Å) for the relevant O_2^+ and O_2^{2+} states are given in Tab. I and Tab. II, respectively. For convenience of discussion, hereafter in this article, we refer the X, a, and b states to the $X^2\Pi_g$, $a^4\Pi_u$, and $b^4\Sigma_g^-$ of O_2^+, while we refer states $0 - 7$ to the O_2^{2+} states according to Tab. II.

Figure 1 shows the potential energy curves of O_2, O_2^+, and O_2^{2+} to illustrate the SDI process. As a first step, the neutral O_2 tunnel ionizes to the X, a, or b states. Then, while the a and b states are coupled by the laser, the X, a, and b states further tunnel ionize to different O_2^{2+} states. Possible parents of O_2^{2+} states from the second tunnel ionization are shown in the last column of Tab. II. Finally, while the newly formed states 1 and 3 dissociate according to their limit in Fig. 1, the other states (except 0) are metastable and dissociate through spin-orbit interaction with other repulsive states [25, 26]. Since the time scale for dissociation through the spin-orbit interaction is much longer than the duration of a femtosecond laser pulse [26], these metastable states could also transfer to other states through laser couplings before dissociation. In particular, we will show in Sec. IV that inclusion of laser couplings between state 6 and states 2 and 3 in the model are crucial to reproduce the experimental KER spectra.

TABLE II. Vertical ionization potential (I_p) to the O_2^{2+} states with two valence holes, calculated in this work. The zero of energy is set to be the zero-point energy of O_2. The calculated energies were systematically shifted such that the $B^3\Pi_g$ state has $I_p = 43.46$ eV. The indexes are arranged according to the KER, which are obtained by subtracting the I_p by the dissociation limit. See the text for computational details.

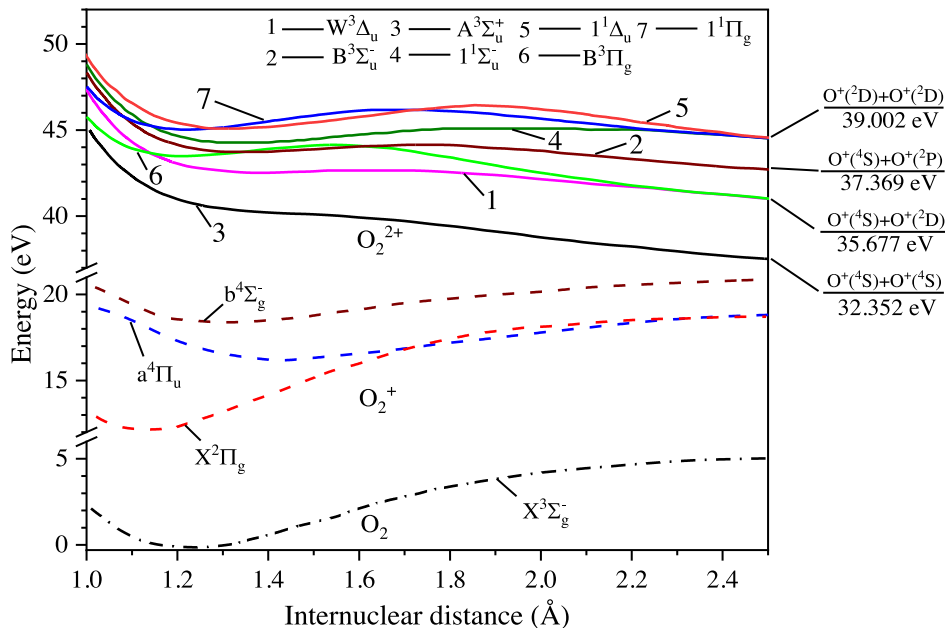| Index	State	Config.	I_p (eV)	Limit	KER (eV)	Parents
0	$X^1\Sigma_g^+$	$1\pi_g^{-2}$	37.19	metastable	–	$X^2\Pi_g$
1	$W^3\Delta_u$	$1\pi_u^{-1}1\pi_g^{-1}$	43.08	$O^+(^4S) + O^+(^2D)$	7.40	$X^2\Pi_g, a^4\Pi_u$
2	$B^3\Sigma_u^-$	$1\pi_u^{-1}1\pi_g^{-1}$	44.20	$O^+(^4S) + O^+(^2D)$	8.52	$X^2\Pi_g, a^4\Pi_u$
3	$A^3\Sigma_u^+$	$1\pi_u^{-1}1\pi_g^{-1}$	41.26	$O^+(^4S) + O^+(^4S)$	8.91	$X^2\Pi_g, a^4\Pi_u$
4	$1^1\Sigma_u^-$	$1\pi_u^{-1}1\pi_g^{-1}$	44.65	$O^+(^4S) + O^+(^2D)$	8.97	$X^2\Pi_g$
5	$1^1\Delta_u$	$1\pi_u^{-1}1\pi_g^{-1}$	45.42	$O^+(^4S) + O^+(^2D)$	9.74	$X^2\Pi_g$
6	$B^3\Pi_g$	$3\sigma_g^{-1}1\pi_g^{-1}$	43.46	$O^+(^4S) + O^+(^4S)$	11.11	$X^2\Pi_g, b^4\Sigma_g^-$
7	$1^1\Pi_g$	$3\sigma_g^{-1}1\pi_g^{-1}$	45.06	$O^+(^4S) + O^+(^4S)$	12.71	$X^2\Pi_g$

FIG. 1. Potential energy curves for relevant O_2, O_2^+, and O_2^{2+} states for this study, adopted from Refs. [25, 34]. Note that dissociation limits of states 2 and 4–7 are different from Tab. II since these states dissociate through spin-orbit interactions with other states [25, 26], which are not shown here for brevity. Curve for state 0 is also not shown here since it does not dissociate in the considered time scale.

TABLE III. Effective binding energies of the spin-up orbitals of the X state and its structure parameters, assuming the remaining electron in the $1\pi_g$ orbital is spin-down. The notation for structure parameters follows Tab. I.

Orbitals	I_p (eV)	l	C_{lm}
$1\pi_g$	24.88	{2, 4}	{1.63, 0.21}
$1\pi_u$	30.60	{1, 3, 5}	{3.26, 0.87, 0.10}
$3\sigma_g$	32.86	{0, 2, 4}	{6.29, 4.70, 0.76}

B. Assignment of binding energies

While it may be clear on how O_2 SDI proceeds, the remaining challenge in the modeling is to assign binding energies of the ionized orbitals corresponding to a manifold of final states which are degenerate in electronic configu-

ration. Consider the tunnel ionization of the $1\pi_u$ orbital of the X state of O_2^+ and assume the remaining electron in the $1\pi_g$ orbital is spin-down. Then, ionizing from another spin-up $1\pi_u$ orbital will form a triplet state. From Tab. II, one sees that states $1-3$ are triplet and share the configuration of $1\pi_u^{-1}1\pi_g^{-1}$, but with different ionization potentials. In the conventional approach, binding energy of the ionized orbital is the energy difference between the final and initial states. Then, it implies that there are three different binding energies for the same spin-up $1\pi_u$ orbital of the X state, which does not make sense in the single active electron picture.

Clearly, the splitting of energy levels is due to the relaxation of electrons cloud after ionization. Therefore, the binding energy of the spin-up $1\pi_u$ orbital of the X state should be a weighted sum of ΔE_1, ΔE_2, and ΔE_3, where $\Delta E_i = E_i - E_X$ is the energy difference between

state i and the X state. One way to average the energies is to assume that states $1-3$ are equally likely to be formed. In particular, since state 1 has a 2-fold degeneracy, it should be counted twice. As a result, the effective binding energy is $E_b = \Delta E_1/2 + \Delta E_2/4 + \Delta E_3/4$. Similarly, for states 4 and 5, their effective binding energy is $E_b = \Delta E_4/3 + 2\Delta E_5/3$, since there are only three allowed states for the singlet $1\pi_u^{-1}1\pi_g^{-1}$ configuration ($^1\Sigma_u^+$ is symmetry forbidden). The same averaging scheme was also applied to the ionization from the a state to states $1-3$. For states 0, 6, and 7, their binding energies are simply the energy difference between the final and initial states. As an example, Tab. III shows the effective binding energies as well as the structure parameters of the spin-up orbitals of the X state. The structure parameters are obtained using the method in Ref. [37]. Note that these structure parameters were also used for ionization from the a and b states, as well as for the spin-down orbitals.

Last but not least, despite states $1-3$ have the same binding energy, their ionization rates are different because of the multiplicity. Naively, in consistent with our averaging scheme, for states $1-3$, their ionization rate should be weighted as $W/2$, $W/4$, and $W/4$, where W is the ionization rate with the effective binding energy. However, if one introduces weighting factors for ionization rates, one should do so systematically for all transitions. In our approach, ionization of a π orbitals have a weight of 2, since one can ionize the π_+ or π_- orbitals, while ionization of a σ orbital only has a weight of 1. For ionization to states $1-3$ from the X or a states, their weight for ionization rates should be further multiplied by $1/2$, $1/4$, and $1/4$, such that the final weights for states $1-3$ are 1, $1/2$, and $1/2$. Similarly, for ionization of a π_u orbital from the X state to states 4 and 5, the weighting factors are $2/3$ and $4/3$, respectively.

C. Electronic structure calculations

In the electronic structure calculations of O_2^+ and O_2^{2+}, the internuclear distance is fixed at $R = 1.21$ Å, the electrons in the $1\sigma_g$ and $1\sigma_u$ orbitals are kept frozen, while the active space consists of the orbitals $2\sigma_g$, $2\sigma_u$, $3\sigma_g$, $1\pi_u$, $1\pi_g$ and the unoccupied orbital $3\sigma_u$. We used the ANO-L basis for the O atom and used the state averaged complete active space self consistent field (SAl-CASSCF(m,n)) calculation to obtain the electronic wave functions, where l is the number of states, m is the number of electrons in the active space, and n is the number of active orbitals. We then performed the second-order perturbation (CASPT2) calculation using those wave functions to improve the accuracy of the energies. Note that the calculations were done without enforcing the symmetry of the molecule. These calculations were done using the open source package OpenMolcas [39].

For O_2^+, the vertical ionization potentials for the X, a, and b states are taken from the experimental

TABLE IV. Transition dipole moments between O_2^{2+} states calculated in this work. Note that the dipole moment between $W^3\Delta_u$ and $B^3\Pi_g$ is double counted since both states are doubly degenerate.

State 1	State 2	Dipole moment (a.u.)
$W^3\Delta_u$	$B^3\Pi_g$	$0.318\ \hat{x}$
$B^3\Sigma_u^-$	$B^3\Pi_g$	$0.123\ \hat{x}$
$A^3\Sigma_u^+$	$B^3\Pi_g$	$0.234\ \hat{x}$
$1^1\Sigma_u^-$	$1^1\Pi_g$	$0.126\ \hat{x}$

value [36], but the transition dipole moment between the a and b states was calculated using the SA3-CASSCF(11,8)/CASPT2 method. The calculated excitation energy from the a to b state is 1.42 eV, which is in excellent agreement with the experimental value of 1.5 eV. The transition dipole moment between these two states is found to be $0.29\ \hat{x}$ a.u., which agrees with the result from Ref. [35]. Note that we used the d_x component to represent the transition from both $\Pi_\pm$ states to a Σ state. The only doublet state we considered for O_2^+ is the X state. This is because from the SA6-CASSCF(11,8)/CASPT2 calculation for doublet states, we found that the lowest two $^2\Pi_u$ state, which are 5.56 and 6.98 eV above the X state, consists mainly of configurations with a spin flipped electron in the $1\pi_g$ orbital and cannot be reached from tunnel ionization. Their laser couplings to the X state are negligible due to the large excitation energies. The higher doublet states which can be reached from ionization were not considered, since their ionization potentials are too high (above 20 eV [36]).

For O_2^{2+}, we calculated the energies of the triplet and singlet states using the SA8- and the SA6-CASSCF(10,8)/CASPT2 method, respectively. We set the vertical ionization potential of state 6 ($B^3\Pi_g$) to be 43.46 eV, as it was done in the fitting of O_2 normal Auger spectrum in Ref. [27]. Then, the energies of all other triplet and singlet states are shifted systematically, and the results are shown in Tab. II. Our vertical ionization potential of state 1 ($W^3\Delta_u$) and 2 ($B^3\Sigma_u^-$) are in excellent agreement with the fitted energies in Ref. [27], which were found to be 43.05 and 44.2 eV. The potential of state 3 ($A^3\Sigma_u^+$) and the other singlet states also seems to agree with the potential energy curves at $R = 1.21$ Å in Ref. [25]. The calculated transition dipole moments between relevant states are tabulated in Tab. IV.

III. MAIN RESULTS

To simulate the KER spectrum and compare it with the experiments from Voss *et al.* [13] and Wu *et al.* [24], we used a linearly polarized Gaussian laser pulse with peak intensity at 1.2×10^{15} W/cm^2, central wavelength of 800 nm, and pulse duration of 8 fs. After solving Eq. (1), populations of the O_2^{2+} states at different alignment angles are obtained and averaged with an isotropic distribu-

tion. The KER spectrum is then calculated by convolving the angular averaged yield with Gaussian functions with an energy resolution of 0.4 eV [12].
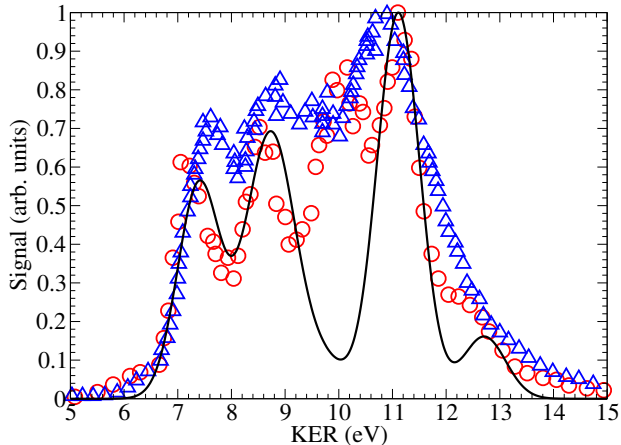

FIG. 2. Comparison of kinetic energy release spectra of $O^+ + O^+$ from Voss *et al.* [13] (red circles), Wu *et al.* [24] (blue triangles), and our model with a 800 nm linear polarized Gaussian laser pulse with peak intensity at 1.2×10^{15} W/cm^2 and pulse duration of 8 fs (black line). The 11 eV peaks are all normalized to unity.

Figure 2 shows the KER spectra of $O^+ + O^+$ from Voss *et al.* [13], Wu *et al.* [24], and our model. All KER spectra are normalized to unity at the highest peak. The spectrum from Wu *et al.* is shifted by 0.8 eV to higher energies to match the results from Voss *et al.*. Overall, the agreement between the two experiments and the theory are excellent, despite the wavelength and intensity of the laser used by Wu *et al.* was reported to be 780 nm and 1×10^{15} W/cm^2. Positions of the first three peaks at around 7.4, 8.8, and 11 eV agree very well between the three results. These peaks are in an increasing order in all three spectra, but the spectrum from Wu *et al.* have slightly larger values for the first two peaks.

On the down side, the spectra from Voss *et al.* and Wu *et al.* have some structures around 10 eV, while our spectrum has a sharp minimum. One can also see that width of the 11 eV peak from Voss *et al.* and Wu *et al.* are different, most likely because the two experiments have different energy resolutions. While there is a sharp peak at 10 eV in the spectrum from Voss *et al.*, the structure around 10 eV in the spectrum from Wu *et al.* does not appear as a peak. [24]. As a result, it is not clear whether there is indeed a peak at around 10 eV.

In short, we found that the KER spectrum simulated by our model reproduces the main features of the KER spectra by Voss *et al.* [13] and Wu *et al.* [24]. The agreement between the results are excellent, suggesting that the assumptions made in the DM-SDI model are valid, particularly the averaging of binding energies.

IV. MECHANISMS OF O$_2$ SDI

In this section, we will explore the mechanism behind O$_2$ SDI. We will first assign the KER peaks to different O_2^{2+} states and then discuss the effects of laser couplings on each peak. Next, we will discuss orbital relaxation of ionized orbitals and the degenerate electronic configuration in some O_2^{2+} states. The laser parameters used in this section are the same as in Fig. 2.
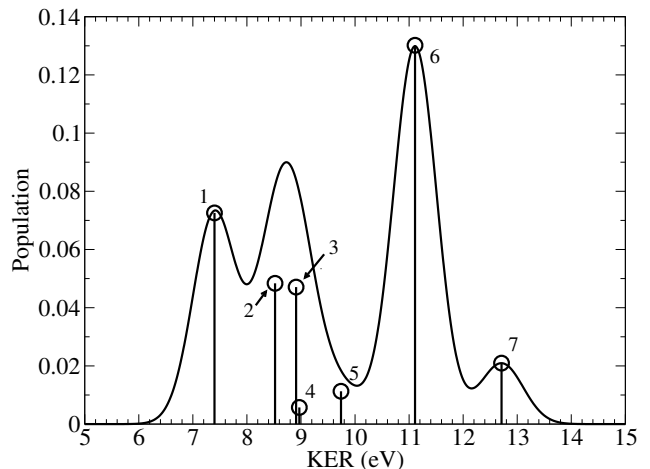
A. Assignment of KER peaks

FIG. 3. Population of different O_2^{2+} states labeled according to Tab. II and the convoluted KER spectrum as in Fig. 2.

Figure 3 shows the assignment of KER peaks to different O_2^{2+} states according to Tab. II. The assignment can be summarize as follows:

7.4 eV peak – state 1 ($W^3\Delta_u$).
8.8 eV peak – states 2 ($B^3\Sigma_u^-$) and 3 ($A^3\Sigma_u^+$).
11 eV peak – state 6 ($B^3\Pi_g$).
12.7 eV peak – state 7 ($1^1\Pi_g$).
Weak signals – states 4 ($1^1\Sigma_u^-$) and 5 ($1^1\Delta_u$).

While our assignment of the 7.4 and 11 eV peaks agree with Voss *et al.* and Wu *et al.*, there are disagreements on the assignment of the 8.8 eV peak. Our calculation suggests that state 3 contributes substantially to the 8.8 eV peak, but this state was not considered in their work. We found that the population of states 4 and 5 are small, therefore these states do not contribute to the 8.8 eV peak, in contrast to their assignment.

Since the contribution from state 5 to the KER spectrum is small, our spectrum has a sharp minimum instead of a peak around 10 eV. To see what could contribute to the structure around 10 eV in the experiment, first we observe that the small peak at 12.7 eV was not resolved in the experiments by Voss *et al.* and Wu *et al.*. This suggests that there could be a broadening effect due to the vibrational motion of neutral molecule, which was also speculated in the study of N$_2$ SDI [12]. Consequently,

the structure around 10 eV could come from the 8.8 and 11 eV peak, and the additional structure would come from SDI to state 5. However, it is beyond the scope of this work to study the vibrational broadening effect, which we intend to address in the future.

If there is a genuine peak at 10 eV, then it means there are missing contributions to the KER spectrum. Since we consider the lowest 6 singlet and triplet states of O_2^{2+}, one may think that quintet states could contribute to the spectrum. However, from our SA3-CASSCF(10,8)/CASPT2 calculations for the quintet states, the $1^5\Sigma_g^+$ and $1^5\Pi_u$ states have vertical ionization potentials of 45.5 and 46.9 eV. Since they dissociate to $O^+(^4S) + O^+(^4S)$ and $O^+(^4S) + O^+(^2D)$ respectively [25], that means their KER are 13.2 and 11.2 eV, which cannot contribute to the 10 eV structure.

The remaining possibility is that some other processes with comparable contribution to SDI lead to formation of state 5. One possible process is the nonsequential double ionization (NSDI). In the experiment by De *et al.* [21], using a 790 nm, 8 fs, and 4×10^{14} W/cm^2 laser, they observed a peak around 10 eV in the KER spectrum of $O^+ + O^+$ and assigned it to state 5. At this laser intensity, state 5 is mostly likely to be formed by NSDI. While it is unlikely for NSDI to have comparable contribution to SDI at the peak intensity of 1.2×10^{15} W/cm^2, no conclusion can be drawn at this time, unless there are additional experimental data on strong field double ionization of O_2 or theoretical study on NSDI of O_2.
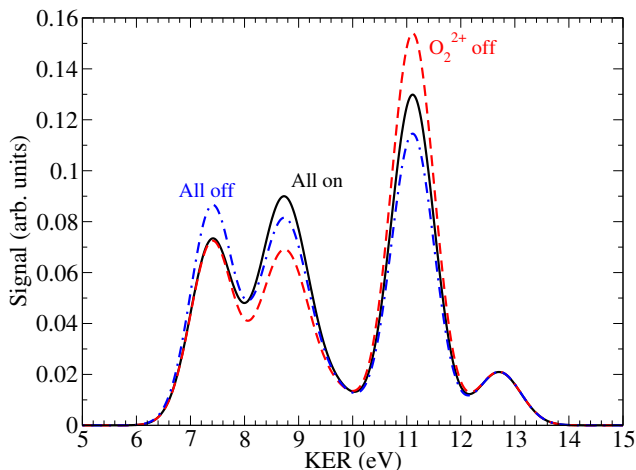
B. Effects of laser couplings

FIG. 4. Effects of laser couplings between O_2^+ states and O_2^{2+} states on the KER spectrum. Black: All laser couplings are on. Red: Laser couplings between O_2^{2+} states are off. Blue: All laser couplings are off. Laser parameters are the same as in Fig. 2.

One important extension of the DM-SDI model [12] to O_2 is to include the laser couplings between the O_2^{2+}

states. To examine the role of these couplings, we solved Eq. (1) with dipole moments between O_2^{2+} states set to zero, i.e. switching off the O_2^{2+} laser couplings. The black solid line and red dashed line in Fig. 4 show the KER spectra with and without the O_2^{2+} laser couplings. Without the couplings, the 8.8 eV peak becomes slightly lower than the 7.4 eV peak, and the 11 eV peak becomes higher. This is because the role of O_2^{2+} laser couplings is to transfer the population from state 6 to states 2 and 3. After switching off the couplings, the sum of yield of states 2 and 3 is equal to the yield of state 1, since states 1 – 3 share the same binding energy in our model. Therefore, after the convolution, the 8.8 eV peak becomes slightly lower than the 7.4 eV peak. As a result, one can see that laser couplings can still play a role after reaching to the doubly charged states in the SDI process.

It is also of interests to investigate the importance of laser coupling between the a and b state of O_2^+. The blue dotted-dashed line in Fig. 4 shows the KER spectrum when all laser couplings are switched off. It is instructive to compare the result with the spectrum without O_2^{2+} couplings (red dashed line). We see that the 11 eV peak drops significantly when the O_2^+ coupling is also turned off. Since state 6 is formed from the X or b state (see Tab. II) and the X state does not couple to the a and b states, this implies that transient population of the b state is decreased with the switch off of the O_2^+ laser coupling. This also implies that the transient population of the a state increases, such that the 7.4 and 8.8 eV peaks are higher. Hence, further turning off the O_2^+ laser coupling causes the KER spectrum further deviates from the qualitative behavior of the experimental spectra.

We have thus showed that the laser couplings between O_2^+ states and O_2^{2+} states are crucial to reproduce all the qualitative behavior of the experimental KER spectra. It is not unexpected that laser couplings between the doubly charged states are still relevant in SDI. This means that one may not simulate all the details of the dissociation dynamics of doubly charged states in SDI simply by propagating classical trajectories with a field-free Hamiltonian. In addition, O_2 SDI is a good example of complicated systems where doubly charged states could dissociate through interactions with other repulsive states. Such dissociation dynamics requires significant theoretical effort to understand and therefore greatly increases the difficulties in modeling SDI. Similar post-ionization dynamics have been recently studied in NSDI of OCS [40].

C. Orbital relaxation

After ionization, the remaining occupied valence orbitals will relax and become more localized in space, such that the ionization potentials are increased. In our previous approach [12], we assumed that the structure parameters C_{lm} of orbitals of the neutral and the ionic states are identical, but the ionization potentials are different. In this section, we examine the changes in C_{lm} due to or-
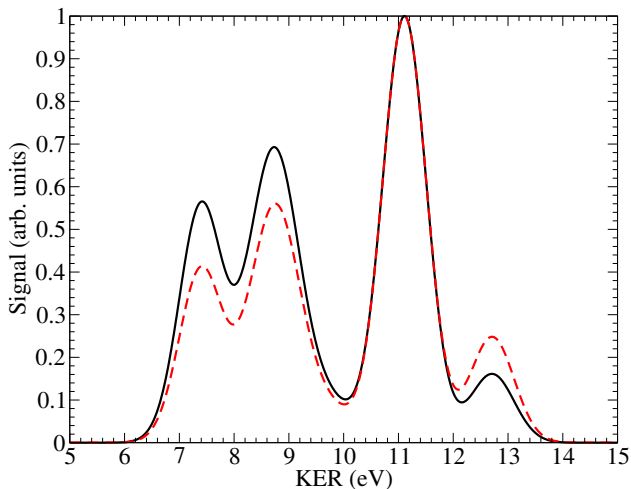
FIG. 5. Normalized KER spectrum calculated using the structure parameters of O_2 and O_2^+ (solid line) and using only the structure parameters of O_2 (dashed line). Laser parameters are the same as in Fig. 2.
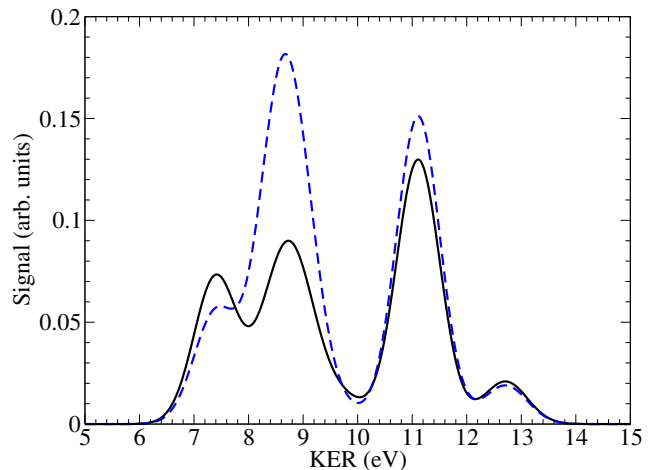

FIG. 6. KER spectra simulated by the model used in Fig. 2 (solid line) and the Dyson model (dashed line). Laser parameters are the same as in Fig. 2. See the text for details about the Dyson model.

bitals relaxation after ionization, as well as its influence on the qualitative behavior of the KER spectrum of O^+ + O^+.

Figure 5 shows the simulated KER spectra using the structure factors of O_2 and O_2^+ and using only the structure factors of O_2. We found that when using only the structure factors of O_2, the values of the 8.8 eV and 7.4 eV peaks are smaller, but the qualitative behavior of the KER spectrum remains: the first three peaks are in an increasing order. This is because the largest component of C_{lm} (see Tab. III and Tab. I) remains the same and the ratios between components for different orbitals are similar. That leads to similar angular dependence of the ionization rates, and thus similar qualitative behavior of the spectrum.

Another change in structure parameters to consider is the orbital relaxation after excitation. We obtained the structure parameters of the $1\pi_g$ orbital of the a state and the b state separately by the method of Zhao *et al.* [37], where the electron density of the excited states is represented by changing only the occupation numbers of the orbitals. Using these structure parameters for the a and b state [41], we found that the ratio between KER peaks change by less than 5% compared to the solid line in Fig. 5. Therefore, one can neglect the changes in structure parameters due to orbital relaxation after excitation.

To summarize, we found that using only the structure parameters of the neutral molecule does not have influence on the qualitative behavior of the KER spectrum of O^+ + O^+. It is an important result because it justified the assumption we made in our previous model for N_2 SDI. It also allows us to keep the SDI model simple, such that it is possible to extend the model to more complicated systems and scenarios.

D. Degenerate electronic configuration

In Sec. II, we discussed the ambiguity of assigning binding energies to the $1\pi_u$ or $1\pi_g$ orbitals of the X or a states. Assuming the final states are degenerate (in terms of electronic configuration), we averaged out the vertical ionization potentials according to their multiplicity and obtained an effective binding energy. Then, in Sec. III, we showed that our model reproduced the qualitative behavior of the experimental KER spectra. In this section, we adapt a many-electrons model for tunneling ionization and compare the simulated KER spectrum to the one in Fig. 2.

To account for the many-electrons effect, one typically uses the so-called Dyson orbitals, which is the overlap of the N- and $(N-1)$-electrons wave functions, to replace the Hartree-Fock or Kohn-Sham orbitals in tunneling ionization models [42]. This implies that the Dyson orbitals from the same initial but different final states are different. Consequently, ionization from the X state to states $1-3$ have three different ionized orbitals. To implement this approach to the SDI model, we first note that the shape of these Dyson orbitals are strikingly similar to the Hartree-Fock orbitals, such that it is reasonable to approximate the structure parameters of the Dyson orbitals by the parameters in Tab. III. The binding energy of these Dyson orbitals is taken as the energy difference between the final and initial states. The weighting factors for ionization rates then follows the rule for π or σ orbitals, as discussed in Sec. II. In fact, this approach was used in modeling N_2 SDI by our previous work (without the weighting factors) [12]. For convenience of the following discussion, we called this model the Dyson model.

Figure 6 compare the simulated KER spectra by the model used in Fig. 2 and the Dyson model. One can immediately see that the qualitative behavior of the spec-
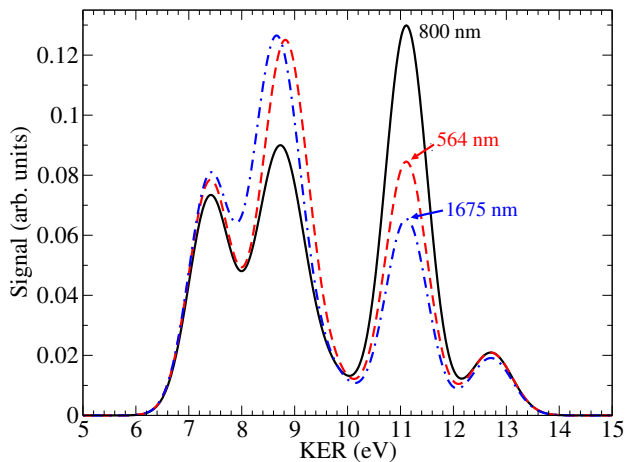
FIG. 7. Angular averaged yield of O_2^{2+} and KER spectra at different wavelengths: 800 nm (black), 564 nm (red), and 1675 nm (blue). Other laser parameters are the same as in Fig. 2.
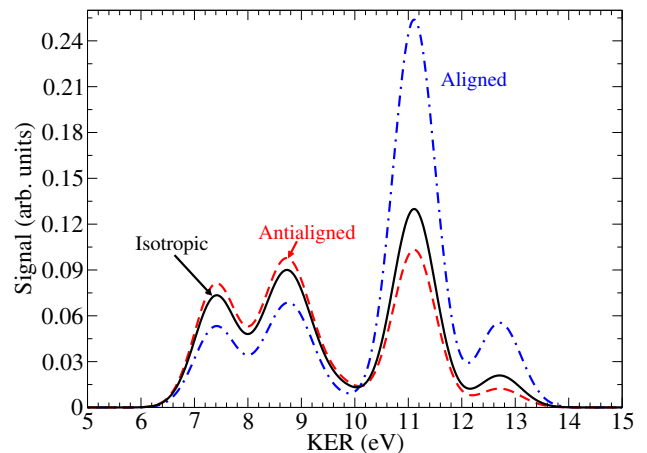

FIG. 8. Effects of alignment on the KER spectrum. Laser parameters are the same as in Fig. 2. See the text for details about the alignment distribution functions.

trum simulated by the Dyson model is not consistent with the experimental spectra. Namely, the 8.8 eV peak is more prominent than the 11 eV peak. This happens because the binding energies of Dyson orbitals for states $1 - 3$ are different. Consequently, the ionization rates to states 3 becomes the largest among states $1 - 3$ due to its low vertical ionization potential. The discrepancy in the qualitative behavior of the simulated spectrum strongly suggests that there should be one binding energy instead of three for the ionization to states $1 - 3$. Therefore, while the use of Dyson model works well for N_2 [12], the same model does not apply to O_2 SDI.

From the comparison of the two different models, we arrive to the conclusion that the single active electron picture with effective binding energies captures the physics better than the Dyson model we defined earlier. The averaging scheme we proposed for the effective binding energy is quite general, and we expect that it can be applied to similar situations for other systems. This would allow us to continue the study of SDI for complex targets using the current model.

V. EFFECTS OF LASERS ON THE KER SPECTRA

In this section, we explore how the KER spectrum of $O^+ + O^+$ will change with different central wavelengths of the laser, different alignments between the laser polarization and the molecular axis, and different peak laser intensities. Unless otherwise specified, the laser parameters used in this section are the same as in Fig. 2.

A. Wavelength dependence

In the previous section, we have seen the importance of laser couplings in O_2 SDI, so one expects that changing the central wavelength of the laser would also have impact on the KER spectrum. It would be particularly interesting to use a 564 nm and a 1675 nm laser, since their frequencies (2.2 and 0.74 eV) would drive states 3 and 6 and states 2 and 6 in resonance, respectively.

Figure 7 shows the KER spectra calculated using central wavelength of 800 nm, 564 nm, and 1675 nm. We see that the use of 564 nm and 1675 nm laser greatly enhance the 8.8 eV peak but suppress the 11 eV peak for both wavelengths. This is expected since the resonance conditions would enhance the population transfer from state 6 to states 2 or 3. We suggest future experiments on O_2 SDI to be carried out at similar wavelengths, since such sharp changes in the qualitative behavior of the spectra should be easily detected in experiments. Then, the results can further test the DM-SDI model and could confirm that the KER spectrum of $O^+ + O^+$ from SDI can be effectively controlled by changing the central wavelength of the laser, as it was done for nonsequential double ionization of O_2 by Alnaser et al. [17].

B. Alignment dependence

Since laser alignment of O_2 has been achieved experimentally, it would also be interesting to investigate the alignment dependence of the KER spectrum of $O^+ + O^+$. A recent study by Wangjam et al. [43] showed that it is possible to align and antialign the O_2 molecule with $\langle \cos^2 \theta \rangle$ about 0.7 and 0.2, respectively. Therefore, we simulated the KER spectrum with alignment distribution functions $\propto \cos^6 \theta$ and $\propto \cos^2(\theta - \pi/2)$, which have $\langle \cos^2 \theta \rangle$ about 0.77 and 0.2, respectively.
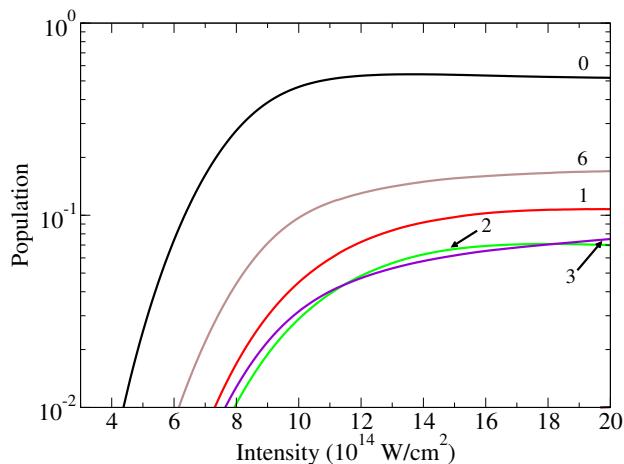
FIG. 9. Intensity dependence of the angular averaged yield of the major O_2^{2+} states. Other laser parameters are the same as in Fig. 2.
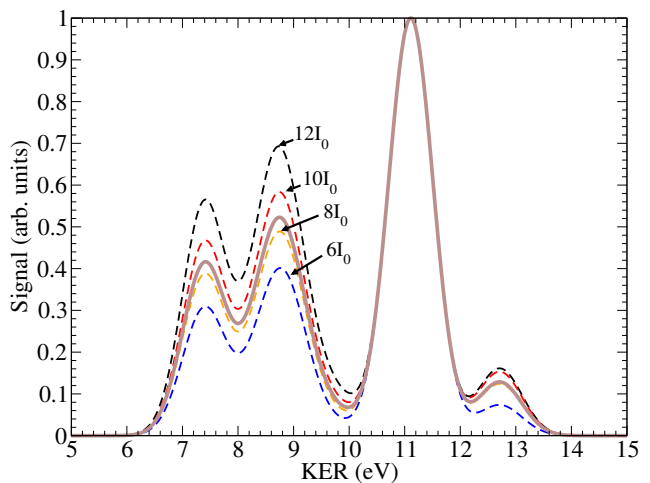

FIG. 10. Normalized KER spectra at different laser intensities (thin dashed lines) and the volume-averaged spectrum with peak intensity at $12I_0$ (thick solid line), where $I_0 = 10^{14}$ W/cm^2. Other laser parameters are the same as in Fig. 2.

Figure 8 shows the KER spectra with aligned, antialigned, and isotropic O_2. We see that the spectrum for aligned O_2 has a very sharp peak at 11 eV compared to isotropic O_2, while the 7.4 eV and 8.8 eV peaks of the aligned O_2 spectrum are weaker than the isotropic O_2 spectrum. This can be explained by the MO-ADK theory and by the effects of laser couplings. At 0 or 180 degrees, ionization of the $1\pi_u$ orbital is suppressed, while ionization of the $3\sigma_g$ orbital is enhanced. In addition, since all transition dipole moments are perpendicular to the molecular axis (see Sec. II), laser couplings are suppressed for aligned O_2. Hence, yield of states $1-3$ decrease and yield of state 6 increases. On the other hand, the KER spectrum with antialigned O_2 does not change significantly compared to the isotropic one, since the degree of antialignment is weak.

We have shown here that experimentally accessible alignment condition for O_2 can greatly alter the qualitative behavior of the KER spectrum of $O^+ + O^+$. To further validate our model, it is highly desirable to have new measurement for the KER spectrum in pump-probe experiments for O_2, where the pump laser aligning the molecule and the probe laser triggering SDI of the molecule.

C. Intensity dependence

Taking advantage of the low computational cost of our model, in this section, we investigate the intensity dependence as well as the focal volume effect in O_2 SDI. To simplify the notation, we define the unit I_0 here as 10^{14} W/cm^2.

Figure 9 shows the intensity dependence of angular averaged yield of states $0-3$ and 6, which are the most populated O_2^{2+} states. For all intensities, we see that yield of state 0 is the highest, followed by the yield of

state 6. The yield of states $1-3$ are similar since they share the same effective binding energy. Yield of all these states start to saturate at intensity about $11I_0$, suggesting that there is no need to go above that laser intensity in the experiment.

Figure 10 shows the variation of KER spectra with different peak laser intensities and the effect of volume averaging [44]. These spectra have similar qualitative behavior, but the 11 eV peak is increasingly dominant at lower intensity, as can be seen from the spacing between state 6 and states $1-3$ in Fig. 9. Therefore, volume averaging would bring down the ratios between the peaks, but retaining the qualitative behavior of the spectra. The volume averaged spectrum with peak intensity at $12I_0$ is showed as the thick solid line in Fig. 10. Indeed, the spectrum lies between the spectra at different peak intensities and shows similar qualitative behavior.

From comparing the KER spectra calculated at different peak intensities, we see that the ratios between the peaks could vary by about $\pm 20\%$ when the peak intensities vary also by $\pm 20\%$, which is within the range of typical uncertainties in laser diagnostics in experiments. This suggests that, once again, we should focus on the qualitative behavior of the KER spectrum from SDI rather than the quantitative aspects. Therefore, in this sense, one can conclude that the focal volume effect does not play an important role in O_2 SDI in the considered range of laser intensity.

VI. SUMMARY AND OUTLOOK

To summarize, we have extended the DM-SDI model developed recently [12] to the open-shell diatomic molecule O_2. The major extensions of model are the inclusion of laser couplings between doubly charged states

and the introduction of effective binding energies in the case of degenerate electronic configuration. We simulated the KER spectrum of $O^+ + O^+$ using the extended DM-SDI model and obtained excellent qualitative agreement with the experimental spectra from Voss *et al.* [13] and Wu *et al.* [24]. Taking advantage of the low computational cost, we explored the physics behind O_2 SDI and different effects of the lasers on the KER spectrum. While we made several assumptions in the DM-SDI model, it appears that those assumptions are valid in the SDI process initiated by an ultrashort (< 10 fs) intense IR laser pulse.

Based on the comparison of experimental and theoretical KER spectra presented in this article on O_2 and in the previous article on N_2 [12], it is fair to say that the DM-SDI model first presented by Yuen and Lin [12] has successfully explained the existing experimental data on dissociative sequential double ionization of simple diatomic molecules by ultrashort intense IR lasers, even though those experiments were carried out decades before. A key feature of the model is that many-body electronic wave functions are not involved explicitly. The model only requires static electronic structure information calculated using those wave functions, such as vertical ionization potentials, transition dipole moments, and structure parameters for valence orbitals. Therefore, computational cost of DM-SDI is very low. Consequently, calculations for different molecular orientation with respect to the laser, different wavelengths, and different laser intensities can all be readily carried out, such that the theoretical results can be compared directly to experiments. This is in sharp contrast to calculations carried out using quantum chemistry packages, where a single calculation is already computationally costly.

From the experimental sides, most of the SDI experiments have been carried out at least a decade ago using longer pulses for many molecules. However, the use of long pulses make observables difficult to interpret, since nuclei motion could be important during the ionization process and there could be subsequent ionization of neutral fragments from large molecules. Today, sub-ten femtosecond lasers of various wavelengths are widely available, and many molecules also can be aligned or oriented. In view that DM-SDI has been shown to predict alignment, laser intensity, and wavelength dependence, it would be desirable that more experiments to be carried out to test the predictions according to the DM-SDI which can be provided by the authors. In particular, alignment and wavelength dependence would be a sensitive test as demonstrated in Sec. V.

Looking ahead, we anticipate to further develop the DM-SDI model along several directions. One direction is to apply the model to larger molecules. Since many-body electronic wave functions are not involved explicitly in DM-SDI, its computational cost does not scale with number of electrons and size of a molecule. However, the major challenge for applying DM-SDI for large molecules is on the determination of dissociation dynamics of doubly charged states. In O_2 SDI, a few O_2^{2+} states are metastable and they would couple to other dissociative states by spin-orbit or laser couplings to dissociate to different limits. While in N_2 SDI [12], the relevant doubly charged states are either stable (N_2^{2+} could be detected) or repulsive. From these two examples, one can see that dissociation dynamics varies greatly for different molecules. Attempts to do full dissociation dynamics from first principles calculations would be extremely complex, for example, see the case of H_2O^{2+} [45]. As the size of the molecule increases, theoretical determination of dissociation dynamics would become even more challenging as there will be more fragmentation channels [6, 9, 10]. Nevertheless, it is possible to reduce the computational effort on the dissociation dynamics calculations by reducing the number of considered doubly charged states. This can be done by calculating SDI yield of different states using DM-SDI and neglecting those states with small yield.

Another direction we have in mind is to use KER spectra via dissociative SDI for molecular dynamics imaging. In general, imaging is an inverse scattering problem which requires many iterative computations. Therefore, to retrieve molecular structure or dynamics, the underlying theory should be simple and have low computational cost. Some examples are the high harmonic spectroscopy [46, 47] and laser-induced electron diffraction [48, 49] using the quantitative rescattering model. We believe that DM-SDI also has the simplicity to perform iterative retrieval calculations without significant computational effort. Starting with a pump pulse to create an excited wave packet, we suggest to use an ultrashort intense IR laser pulse to doubly ionize the excited wave packet and measure the KER at different time delays of the probe pulse. Using the KER spectra at different delays, it is possible to retrieve the excited wave packet initiated by the pump pulse by using DM-SDI and some optimization algorithms. This idea will have to be tested out with further simulations and realization using experimental data. We will demonstrate the feasibility of this scheme in our upcoming work.

Finally, we would like to comment on the NSDI yield versus the SDI yield. In experiments, different laser intensities inside the focal volume would contribute to the double ionization. At lower intensities ($\sim 10^{14}$ W/cm^2), one expects that NSDI would be the dominant process. However, since NSDI is challenging to model, to examine the importance of NSDI in the entire focal volume, one may rely on experimental effort. One possible approach is to investigate the intensity dependence on doubly charged to singly charged yield ratio and identify the SDI regime (the knee structure), similar to the seminal work on strong field double ionization of He [50]. Another approach would be to compare the measured KER spectra using linearly polarized and circularly polarized laser (with the same peak field strength) [13]. There should be a range of peak laser intensities where the NSDI yield is negligible compared to SDI, such that the DM-SDI model

can be used to simulate double ionization of the target in the entire focal volume.

[1] C. Beylerian and C. Cornaggia, J. Phys. B: At. Mol. Opt. Phys. **37**, L259 (2004).

[2] Z. Wu, C. Wu, X. Liu, Y. Deng, Q. Gong, D. Song, and H. Su, J Phys Chem A **114**, 6751 (2010).

[3] J. Wu, L. P. H. Schmidt, M. Kunitski, M. Meckel, S. Voss, H. Sann, H. Kim, T. Jahnke, A. Czasch, and R. Dörner, Phys. Rev. Lett. **108**, 183001 (2012).

[4] X. Xie, K. Doblhoff-Dier, H. Xu, S. Roither, M. S. Schöffler, D. Kartashov, S. Erattupuzha, T. Rathje, G. G. Paulus, K. Yamanouchi, A. Baltuska, S. Grafe, and M. Kitzler, Phys. Rev. Lett. **112**, 163003 (2014).

[5] S. Zhao, B. Jochim, P. Feizollah, J. Rajput, F. Ziaee, P. KanakaRaju, B. Kaderiya, K. Borne, Y. Malakar, B. Berry, J. Harrington, D. Rolles, A. Rudenko, K. D. Carnes, E. Wells, I. Ben-Itzhak, and T. Severt, Phys. Rev. A **99**, 053412 (2019).

[6] N. Iwamoto, C. J. Schwartz, B. Jochim, K. Raju P, P. Feizollah, J. Napierala, T. Severt, S. Tegegn, A. Solomon, S. Zhao, H. Lam, T. N. Wangjam, V. Kumarappan, K. D. Carnes, I. Ben-Itzhak, and E. Wells, J. Chem. Phys. **152**, 054302 (2020).

[7] G. Basnayake, P. Hoerner, B. Mignolet, M. K. Lee, Y. F. Lin, A. H. Winney, D. A. Debrah, L. Popaj, X. Shi, S. K. Lee, H. Bernhard Schlegel, F. Remacle, and W. Li, Phys. Chem. Chem. Phys. **23**, 23537 (2021).

[8] C. Cheng, Z. L. Streeter, A. J. Howard, M. Spanner, R. R. Lucchese, C. W. McCurdy, T. Weinacht, P. H. Bucksbaum, and R. Forbes, Phys. Rev. A **104**, 023108 (2021).

[9] T. Townsend, C. J. Schwartz, B. Jochim, T. Severt, N. Iwamoto, J. L. Napierala, P. Feizollah, S. N. Tegegn, A. Solomon, S. Zhao, K. D. Carnes, I. Ben-Itzhak, and E. Wells, Front. Phys. **9**, 691727 (2021).

[10] T. Severt, D. R. Daugaard, T. Townsend, F. Ziaee, K. Borne, S. Bhattacharyya, K. D. Carnes, D. Rolles, A. Rudenko, E. Wells, and I. Ben-Itzhak, Phys. Rev. A **105**, 053112 (2022).

[11] S. Bhattacharyya, K. Borne, F. Ziaee, S. Pathak, E. Wang, A. S. Venkatachalam, X. Li, N. Marshall, K. D. Carnes, C. W. Fehrenbach, T. Severt, I. Ben-Itzhak, A. Rudenko, and D. Rolles, The Journal of Physical Chemistry Letters **13**, 5845 (2022).

[12] C. H. Yuen and C. D. Lin, Phys. Rev. A **106**, 023120 (2022).

[13] S. Voss, A. S. Alnaser, X. M. Tong, C. Maharjan, P. Ranitovic, B. Ulrich, B. Shan, Z. Chang, C. D. Lin, and C. L. Cocke, J. Phys. B: At. Mol. Opt. Phys. **37**, 4239 (2004).

[14] X.-M. Tong, Z. X. Zhao, and C.-D. Lin, Phys. Rev. A **66**, 033402 (2002).

[15] C. Guo, M. Li, and G. N. Gibson, Phys. Rev. Lett. **82**, 2492 (1999).

[16] A. S. Alnaser, S. Voss, X.-M. Tong, C. M. Maharjan, P. Ranitovic, B. Ulrich, T. Osipov, B. Shan, Z. Chang, and C. L. Cocke, Phys. Rev. Lett. **93**, 113003 (2004).

[17] A. S. Alnaser, M. Zamkov, X. M. Tong, C. M. Maharjan, P. Ranitovic, C. L. Cocke, and I. V. Litvinyuk, Phys. Rev. A **72**, 041402(R) (2005).

[18] J. Wu, H. Zeng, and C. Guo, Phys. Rev. A **75**, 043402 (2007).

[19] I. A. Bocharova, A. S. Alnaser, U. Thumm, T. Niederhausen, D. Ray, C. L. Cocke, and I. V. Litvinyuk, Phys. Rev. A **83**, 013417 (2011).

[20] C. Wu, Y. Yang, Z. Wu, B. Chen, H. Dong, X. Liu, Y. Deng, H. Liu, Y. Liu, and Q. Gong, Phys. Chem. Chem. Phys. **13**, 18398 (2011).

[21] S. De, I. A. Bocharova, M. Magrakvelidze, D. Ray, W. Cao, B. Bergues, U. Thumm, M. F. Kling, I. V. Litvinyuk, and C. L. Cocke, Phys. Rev. A **82**, 013408 (2010).

[22] S. De, M. Magrakvelidze, I. A. Bocharova, D. Ray, W. Cao, I. Znakovskaya, H. Li, Z. Wang, G. Laurent, U. Thumm, M. F. Kling, I. V. Litvinyuk, I. Ben-Itzhak, and C. L. Cocke, Phys. Rev. A **84**, 043410 (2011).

[23] B. Gaire, J. McKenna, N. G. Johnson, A. M. Sayler, E. Parke, K. D. Carnes, and I. Ben-Itzhak, Phys. Rev. A **79**, 063414 (2009).

[24] Z. Wu, C. Wu, X. Liu, Y. Liu, Y. Deng, and Q. Gong, Opt. Express **18**, 10395 (2010).

[25] M. Lundqvist, D. Edvardsson, P. Baltzer, M. Larsson, and B. Wannberg, J. Phys. B: At. Mol. Opt. Phys. **29**, 499 (1996).

[26] D. Edvardsson, S. Lunell, F. Rakowitz, C. M. Marian, and L. Karlsson, Chem. Phys. **229**, 203 (1998).

[27] Z. Bao, R. F. Fink, O. Travnikova, D. Céolin, S. Svensson, and M. N. Piancastelli, J. Phys. B: At. Mol. Opt. Phys. **41**, 125101 (2008).

[28] M. Magrakvelidze, C. M. Aikens, and U. Thumm, Phys. Rev. A **86**, 023402 (2012).

[29] P. M. Abanador and U. Thumm, Phys. Rev. A **102**, 053114 (2020).

[30] P. M. Abanador, T. Pauly, and U. Thumm, Phys. Rev. A **101**, 043410 (2020).

[31] S. Xue, H. Du, B. Hu, C. D. Lin, and A.-T. Le, Phys. Rev. A **97**, 043409 (2018).

[32] S. Xue, S. Yue, H. Du, B. Hu, and A.-T. Le, Phys. Rev. A **104**, 013101 (2021).

[33] S. Xue, S. Sun, P. Ding, B. Hu, S. Yue, and H. Du, Phys. Rev. A **105**, 043108 (2022).

[34] F. R. Gilmore, J. Quant. Spectrosc. Radiat. Transfer **5**, 369 (1965).

[35] C. M. Marian, R. Marian, S. D. Peyerimhoff, B. A. Hess, R. J. Buenker, and G. Seger, Mol. Phys. **46**, 779 (1982).

[36] P. Baltzer, B. Wannberg, L. Karlsson, M. CarlssonGothe, and M. Larsson, Phys. Rev. A **45**, 4374 (1992).

[37] S.-F. Zhao, C. Jin, A.-T. Le, T.-F. Jiang, and C. D. Lin, Phys. Rev. A **81**, 033423 (2010).

[38] S.-F. Zhao, J. Xu, C. Jin, A.-T. Le, and C. D. Lin, J. Phys. B: At. Mol. Opt. Phys. **44**, 035601 (2011).

[39] I. Fdez. Galvan, M. Vacher, A. Alavi, C. Angeli, F. Aquilante, J. Autschbach, J. J. Bao, S. I. Bokarev, N. A. Bogdanov, R. K. Carlson, *et al.*, J. Chem. Theory Comput. **15**, 5925 (2019).

[40] T. Endo, K. M. Ziems, M. Richter, F. G. Fröbel, A. Hishikawa, S. Gräfe, F. Légaré, and H. Ibrahim, Front. Chem. , 281 (2022).

[41] The binding energies for the $1\pi_g$ orbital of the a and b state are 26.2 and 25.3 eV. Their structure parameters C_{lm} are {1.83, 0.23} and {1.72, 0.24}(cf. Tab. III).

[42] O. I. Tolstikhin, L. B. Madsen, and T. Morishita, Phys. Rev. A **89**, 013421 (2014).

[43] T. N. Wangjam, H. Lam, and V. Kumarappan, Phys. Rev. A **104**, 043112 (2021).

[44] T. Morishita, Z. Chen, S. Watanabe, and C. D. Lin, Phys. Rev. A **75**, 023407 (2007).

[45] Z. L. Streeter, F. L. Yip, R. R. Lucchese, B. Gervais, T. N. Rescigno, and C. W. McCurdy, Phys. Rev. A **98**, 053429 (2018).

[46] A.-T. Le, R. R. Lucchese, S. Tonzani, T. Morishita, and C. D. Lin, Phys. Rev. A **80**, 013401 (2009).

[47] L. He, S. Sun, P. Lan, Y. He, B. Wang, P. Wang, X. Zhu, L. Li, W. Cao, P. Lu, and C. D. Lin, Nat. commun. **13**, 1 (2022).

[48] J. Xu, Z. Chen, A.-T. Le, and C. D. Lin, Phys. Rev. A **82**, 033403 (2010).

[49] C. I. Blaga, J. Xu, A. D. DiChiara, E. Sistrunk, K. Zhang, P. Agostini, T. A. Miller, L. F. DiMauro, and C. D. Lin, Nature **483**, 194 (2012).

[50] B. Walker, B. Sheehy, L. F. DiMauro, P. Agostini, K. J. Schafer, and K. C. Kulander, Phys. Rev. Lett. **73**, 1227 (1994).